Controlled In Situ Seed-Mediated Growth of Gold and Silver Nanoparticles on an Optical Fiber Platform for Plasmonic Sensing Applications

Hariharan Manoharan[1] · Dharanibalaji KC[2] · V. V. R. Sai[1]

Abstract

This study presents an in situ growth technique to develop highly sensitive plasmonic fiber optic sensors with an excellent control over the plasmonic properties of gold (AuNPs) and silver nanoparticles (AgNPs). Here, we exploit the dual functionality of the U-bent fiber optic sensor (FOS) probes, where the probe acts as, firstly, the substrate for nanoparticles' growth and, secondly, an invaluable tool to monitor as well as control the gold and silver seed binding to the surface amine groups and subsequently their growth in real time by means of the evanescent wave absorbance (EWA) spectral response. Au and Ag seeds (< 5 nm) with a peak absorbance at 510 and 390 nm, respectively, were used. The NP growth kinetics from the probes for different seed densities with a peak EWA response of 0.05, 0.1, and 0.15 optical density (OD) were observed in the presence of the respective metal precursor, cetyltrimethylammonium bromide (CTAB), and ascorbic acid. In comparison with AuNP grown FOS, a significant anisotropic growth was observed for AgNP with a redshift and spectral width as high as 215 nm and 425 nm, respectively, for a peak EWA response of 2.0 OD. The localized surface plasmon resonance (LSPR) activity of the AuNPs and AgNP grown FOS probes was evaluated for seed density of 0.1 OD. These proof-of-the-concept studies show significantly high RI sensitivity and surface-enhanced Raman scattering (SERS) enhancement factor for AgNP probes at 15.8 ΔA/RIU (for 22 AgNPs/μm^2) and 1.3×10^7, respectively, in comparison with 18.9 ΔA/RIU (for 1424 AuNPs/μm^2) and 1.1×10^6, respectively, for AuNP FOS probes. In addition, these plasmonic probes were stable in organic solvent (hexane) but its stability was deteriorated in alkaline solution (1 M NaOH).

Keywords Plasmonic fiber optic sensor · Gold and silver nanoparticles · Seed-mediated growth · LSPR · SERS · Chemical stability

Introduction

Plasmonic nanoparticle decorated waveguides act as an excellent platform for bio-/chemical sensing based on localized surface plasmon resonance (LSPR) or surface-enhanced Raman scattering (SERS) phenomena [1]. Optical fibers are one among the most preferred waveguides as they are reliable, portable, affordable, and capable of providing in situ monitoring in real time [2–4]. LSPR-based plasmonic fiber optic sensors (FOS) have been highly promising for a wide range of applications in detecting ultra-low levels of chemical analytes such as biomolecules, pesticides, gases, and vapors as well as measuring quantities like humidity, pH, temperature, and refractive index [5–10]. The recent advancements in micro- and nanofabrication techniques and new developments in optoelectronics have enabled the concept of "lab on fiber" [11]. This concept offers advantages such as low sample volume requirement and cost-effective point of care testing and also eliminates the need for any bulk instrumentation. The performance, adaptability, and deployment of plasmonic FOS is governed mainly by the simplicity of deposition of the nanostructures and control over their size and shape to tailor their plasmonic properties for a specific application of interest [12, 13]. While the top-down approaches (e.g., lithographic techniques)

✉ V. V. R. Sai
vvrsai@iitm.ac.in

1 Biomedical Engineering Laboratory, Department of Applied Mechanics, Indian Institute of Technology Madras, Chennai 600036, India

2 Department of Chemical Engineering, Indian Institute of Technology Madras, Chennai 600036, India

offer advantage to fabricate a desired plasmonic nanostructure with high repeatability for planar waveguides, the bottom-up approaches are more cost-effective and suitable for cylindrical fiber optic waveguides to chemisorb nanostructures of a desired size and shape obtained by wet-chemical synthetic means [14].

Anisotropic nanoparticles are the ideal choice for fabricating a highly sensitive plasmonic FOS [15]. In many instances, anisotropic noble metal nanoparticles such as nanorods, stars, and bipyramids are synthesized by a seed-mediated technique using the metal precursors, site-specific surfactants, and reducing agents in aqueous solution [16, 17]. Cationic surfactant like CTAB is well known to preferentially adhere to certain crystalline planes and direct the shape of anisotropic nanoparticle [18]. In aqueous solution phase, dense CTAB bilayer on the nanoparticle surface is known to impede their chemisorption to a functionalized optical fiber surface and hence poses a key challenge in developing a highly sensitive plasmonic FOS [19]. Prolonged incubation time (more than 24 h) of a substrate in the colloidal solution and low nanoparticle loading density make this immobilization procedure less attractive [20, 21]. Moreover, the excess CTAB in the solution phase has to be removed by laborious centrifugation procedures for effective immobilization [22].

As an alternative to these less-efficient chemisorption-based techniques, an in situ growth of seed nanoparticles immobilized on an optical fiber surface is adopted in this study. Here, the seed nanoparticles are chemically synthesized without any addition of CTAB in aqueous solution and chemisorbed to an amine-functionalized optical fiber. Subsequently, the seeded fiber probe is immersed in a "growth solution" which promotes the deposition of metals directly on the seed particles with CTAB as capping agent. Growth solution used in this study was modified from the established protocol developed by Jana and co-workers [23, 24]. Using this method, the final nanostructures that are grown can be precisely controlled by seed concentration, incubation time and by modulating the growth conditions [25].

In this study, we utilize U-shaped optical fiber for realizing the plasmonic FOS. The U-bent probes are known to exhibit higher evanescent wave absorbance (EWA) and superior refractive index (RI) sensitivities compared with straight fiber probes [26–29]. This study demonstrates the dual functionality of the U-bent probes where the probe acts as the substrate for nanoparticle's growth as well as a valuable tool to real-time monitor the growth by measuring the evanescent wave-based absorbance spectral measurements. Further, the LSPR-based refractive index sensitivity, SERS activity, and chemical stability of the newly fabricated plasmonic FOS were evaluated.

Experimental Methods

Materials

For nanoparticle synthesis, gold (III) chloride trihydrate ($HAuCl_4 \cdot 3H_2O$) was procured from Sigma. Silver nitrate ($AgNO_3$), sodium borohydride ($NaBH_4$), trisodium citrate, and ascorbic acid were procured from Merck, and cetyltrimethylammonium bromide (CTAB) from SRL chemicals, India. All experiments were carried out using deionized (DI) water (Milli-Q, resistivity = 18.2 MΩ cm).

Multimode optical fibers (FT200UMT, numerical aperture = 0.39) with silica core (diameter 200 μm) and polymer cladding were procured from Thorlabs Inc., USA. Fiber optic spectrometer, USB 4000, with a CCD array detector (200 to 1100 nm wavelength range), and halogen light source, HL-2000, from Ocean Optics were used.

U-Bent Fiber Probe Preparation

Silica fibers were cut to a length of 30 cm using a fiber cleaver, and the distal ends were polished using a polishing disc. The buffer and the cladding layers were removed (decladding) over a length of 1 cm in the middle of fiber with the help of a sharp blade. U-shaped fiber probes were fabricated by exposing the decladded region (straight fiber) to a butane flame and manually bending it at ~1000 °C. Subsequently, the U-region (sensor surface) was washed with excess acetone and ethanol followed by DI water. The fiber bend diameter was 1.0 ± 0.2 mm. Fiber probes were examined under an optical microscope to select probes of a desired geometry and confirm complete decladding (Fig. S1, supplementary information). From here on, we refer this newly constructed U-bent fiber as the sensor probe. To generate silanol groups on the silica fiber core surface of the U-bent region, the probes were dipped in piranha solution (70% sulfuric acid + 30% hydrogen peroxide) for 30 min and washed with excess DI water. The cleaned probes were dried at 100 °C for 30 min. Then, the probes were incubated in 1% solution of 3-aminopropyl-triethoxysilane (APTES, prepared in absolute ethanol) for 15 min followed by excess ethanol wash. Loosely bound silane molecules were removed by sonicating the probes in ethanol for 15 min. Later, it was kept in hot air oven for 100 °C (60 min) for curing. Subsequently, the amine-functionalized probes were stored in nitrogen ambience till further use.

Optical Setup

The schematic of the experimental setup is shown in Fig. 1a. Here, one end of the probe was illuminated using a broadband light source (halogen light), and the other end was connected to a fiber optic spectrometer. The data was acquired in real
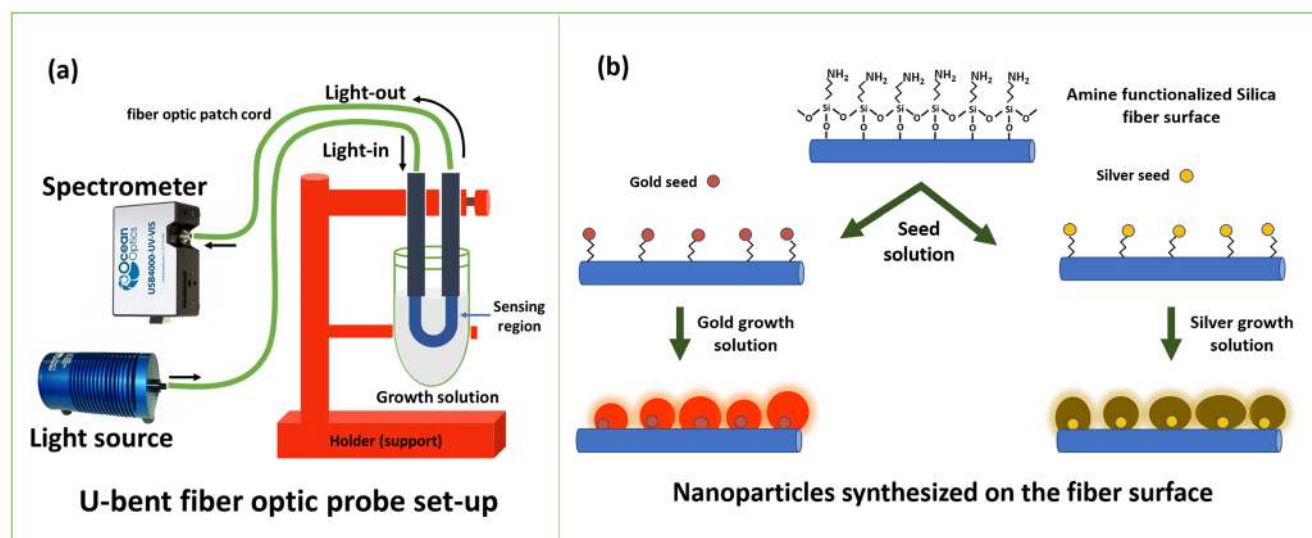
Fig. 1 **a** The experimental setup. **b** Schematic diagram of seed-mediated growth of NPs (silver and gold seeds) on the surface of U-bent fiber probe

time using SpectraSuite software (version 1.6.0_11) with scan averaging between 100 and 200 spectra. The sensing U-region was immersed in a sample holder which contains either seed or growth solution (volume of 500 μl). At the end of measurement, the probe was washed with excess DI water to remove loosely bound particles.

Seed Particle Synthesis

Gold and silver seed nanoparticles were separately synthesized using $NaBH_4$ as strong reducing agent and sodium citrate as capping agent as described below [23, 24]. Firstly, gold seed particles were synthesized taking a 20 ml aqueous mixture containing 0.25 mM $HAuCl_4$ (gold precursor), and 0.25 mM trisodium citrate. To this solution, 0.6 ml of freshly prepared 0.1 M $NaBH_4$ (ice-cold) was added under vigorous stirring conditions. Similarly, for silver seed particle synthesis, $HAuCl_4$ was replaced by $AgNO_3$ (silver precursor) in the abovementioned protocol. The seed particles were used after 5 h.

Seed Immobilization and Nanoparticle Growth

The nanoparticles were grown on amine-functionalized U-bent fiber probes as shown in Fig. S1c (supplementary information). The U-bent fiber probes were incubated in the aqueous seed solution (Au and Ag seeds) diluted by 5 times, which was done mainly to avoid aggregation of the seeds on the probe surface. The seed particles were allowed to chemisorb to the probes until a desired absorbance response is obtained. Subsequently, the probes were taken out of the seed solution and immediately washed thrice with DI water by introducing them into three different vials containing DI water. Concentration of seeds on the fiber probes were controlled by tuning the incubation time. The probes immobilized with

gold or silver seeds were dipped in gold or silver growth solution, respectively. Gold growth solution contained 25 μl $HAuCl_4$ (50 mM), 2.25 ml CTAB (100 mM), and 20 μl ascorbic acid (100 mM), whereas silver growth solution consisted of 32 μl $AgNO_3$ (20 mM), 2.25 ml CTAB (100 mM), 125 μl ascorbic acid (100 mM), and 25 μl NaOH (1 M). The deposition of gold or silver on seed nanoparticles was monitored in real time using a fiber optic spectrometer. The nanoparticles were allowed to grow till the absorbance plasmonic peak wavelength reaches a value of 2.0. Then, the growth of nanoparticles was arrested by taking the probes out of growth solution and washing it with excess of DI water.

Refractive Index Measurements

Sucrose solutions with refractive index (RI) values ranging from 1.333 to 1.348 RI units (RIU) were prepared by dissolving sucrose of different weights in DI water. The final concentrations of these solutions were verified in terms of brix value using a handheld digital refractometer, PAL1 (Atago, Japan) at room temperature.

Raman Scattering Spectroscopy

Nanoparticle grown fiber probes were dipped in 10 mM thiophenol solution prepared in ethanol for 3 h. Then, the probes were washed with excess ethanol and dried under a nitrogen atmosphere. Raman scattering spectra were recorded using a Raman spectrometer (WP 785L, Wasatch Photonics, USA) fitted with f/1.3 collection aperture and a 785-nm laser source under free-space coupling configuration as shown in Fig. 6a. The laser optical power was 100 mW over a spot size of 70 μm on the fiber probe. Raman scattering spectra were recorded using Enlighten™ software.

Chemical Stability Assessment

Freshly prepared plasmonic fiber probes were separately incubated in hexane, HCl (1 M), and NaOH (1 M). The stability was quantified by monitoring the surface plasmon peak of AuNPs and AgNPs for 1 h. For this study, a highly stable white LED light source built in-house was used.

Characterization

For cuvette-based UV-visible spectral measurements, Cary-60 spectrophotometer was used. The size of seeds was determined using FEI Tecnai T20 transmission electron microscopy (TEM). The surface plasmon peak from absorbance graphs was obtained by calculating minimum $dA/d\lambda$ using OriginPro software (edition: b9.5.5.409). The surface morphology was characterized using scanning electron microscopy (SEM, Hitachi 4800), and the energy dispersive X-ray (EDX) technique was used for elemental analysis of the fiber probe surface. Surface coverage of the nanoparticles on the fiber was estimated from SEM images using ImageJ software. Atomic force microscopy (AFM, NX10 Park system) was used to analyze the surface topography and height of the nanoparticles on the FOS.

Results and Discussion

Immobilization of Seed Particles on Fiber Probe Surface

The main objective of this study was to fabricate plasmonic FOS probes using seed-mediated growth of gold (AuNPs) or silver nanoparticles (AgNPs) on the probes' surface. Firstly, colloidal gold (Au) and silver (Ag) seed nanoparticle solutions were prepared separately by reducing $HAuCl_4$ or $AgNO_3$ with $NaBH_4$ in the presence of sodium citrate. From the cuvette-based UV-visible absorption spectral measurements, a plasmon peak at 510 and 390 nm was observed for Au and Ag colloidal seed suspensions, respectively (Fig. S2, supplementary information). TEM images confirmed presence of the seed particles with mean diameter less than 5 nm (Fig. S3, supplementary information). The amine-functionalized (APTES) U-bent fiber probes were dipped separately in either Au or Ag seed solution (Fig. 1b). The seed particles were bound to the amine surface through chemisorption. Evanescent wave absorbance (EWA) technique was utilized to monitor the binding of the seeds at 510 nm and 390 nm for gold and silver nanoparticles, respectively (Fig. 2a,b). During the binding process (within 1 min), absorbance was found to increase with time. When the optical density (OD) reached a value of 0.1, the fiber probe was thoroughly washed with excess DI water to restrict seed binding and remove the loosely bound particles on the probe's surface. This technique enabled us to monitor and control the concentration of seeds on the fiber surface. At OD 0.1, the concentration of Ag seeds will be lower than that of Au seeds because extinction coefficient of silver particles is at least four times higher than that of gold particles at any fixed size [30]. As the seed size was less than 5 nm, we were unable to directly capture the surface coverage of seeds using SEM imaging (Fig. S4, supplementary information).

Seed-Mediated Growth on the FOS Probes

Au- or Ag-seeded fiber probes were subsequently immersed in their respective growth solutions to yield gold (AuNPs) or silver nanoparticles (AgNPs). The immobilized seeds act as the template for nucleation and growth of nanoparticles (NPs). Growth kinetics of NPs was studied by recording EWA-based
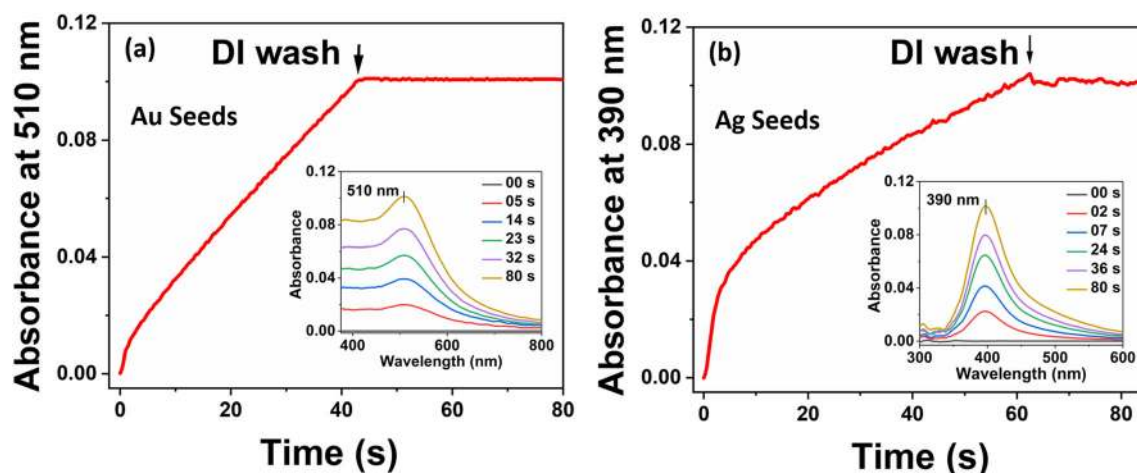

Fig. 2 Binding response of Au or Ag seeds (OD = 0.1) to the amine-functionalized probe was monitored in real time using a fiber optic spectrometer. **a** Au seed binding was recorded at 510 nm and **b** Ag seed binding was recorded at 390 nm. The insets show the EWA-based UV-vis spectra, where absorbance increased with seed binding

UV-vis spectra and monitoring the shifts in surface plasmon peaks in real time. EWA response at the respective characteristic peaks for Au and Ag seeds and the subsequently grown nanoparticles was taken as a measure, in order to be able to compare the plasmonic characteristics of probes obtained with various seed densities after seed immobilization (OD 0.05, 0.1, and 0.15). Similarly, the nanoparticles were allowed to grow until the peak absorbance response reaches 2.0. This absorbance value was chosen mainly due to the constraints on intensity of the light sources used in this study.

Growth of Gold Nanoparticles Au-seeded fiber probes (OD = 0.1 at 510 nm) were dipped in gold growth solution. Figure 3 a shows a steady increase in the EWA spectral response as a result of a rapid AuNP growth over the seed particles. Within 300 s, the peak absorbance response reached a value close to 2.0, and the growth was stopped by washing the fiber with excess DI water. This resulted in a marginal reduction in absorbance as well as a blueshift in the plasmonic peak (from 540 to 535 nm). A resultant redshift of ~ 25 nm (510 to 535 nm) in the LSPR peak was observed. Figure 3 b shows a uniform and proportional rise in the absorbance value at 510, 535, and 600 nm during the AuNP growth, where 535-nm peak remained as the dominant one indicating no considerable shift in the LSPR characteristic peak and thus an isotropic growth in the AuNP. Larger AuNP formation followed by smaller ones was evident from temporal response. AFM image (Fig. S6a, supplementary information) shows that AuNPs

of average height 26 ± 8 nm were formed on the probe surface. Further, from the SEM image (Fig. 3e), the surface coverage of the nanoparticles was found to be 1424 ± 187 particles/ μm^2. A dense and uniform distribution of AuNPs was observed throughout the probe surface (Fig. S5a, supplementary information).

A similar growth pattern was observed in the case of the other seed densities (Fig. 3c). However, after the completion of growth, the plasmonic peak at 546, 535, and 540 nm with a full width at half maximum (FWHM) value of 207, 226, and 252 nm was observed for seed densities of 0.05, 0.10, and 0.15 OD , respectively. The FWHM was found to widen with increase in the seed density, indicating a widening size distribution of the AuNPs after growth. The SEM images (Fig. 3d, f) show the formation of larger nanoparticles with uniform size for 0.05 OD of seed density, while a wider AuNP size distribution in the case of the probes with seed density of 0.15 OD.

Growth of Silver Nanoparticles Similar to AuNP grown FOS, AgNPs were formed on the fiber probe by immersing Ag-seeded probe (OD = 0.1 at 390 nm) in silver growth solution. Under the given experimental conditions, it took about 620 s for silver deposition to reach a peak absorbance of 2.0. The growth was stopped by washing the probe with excess DI water (Fig. 4a). EWA spectra show a significant redshift in the peak wavelength from 390 to 520 nm upon growth of the AgNPs as also depicted in the temporal response (Fig. 4b). AFM image (Fig. S6b, supplementary information) revealed
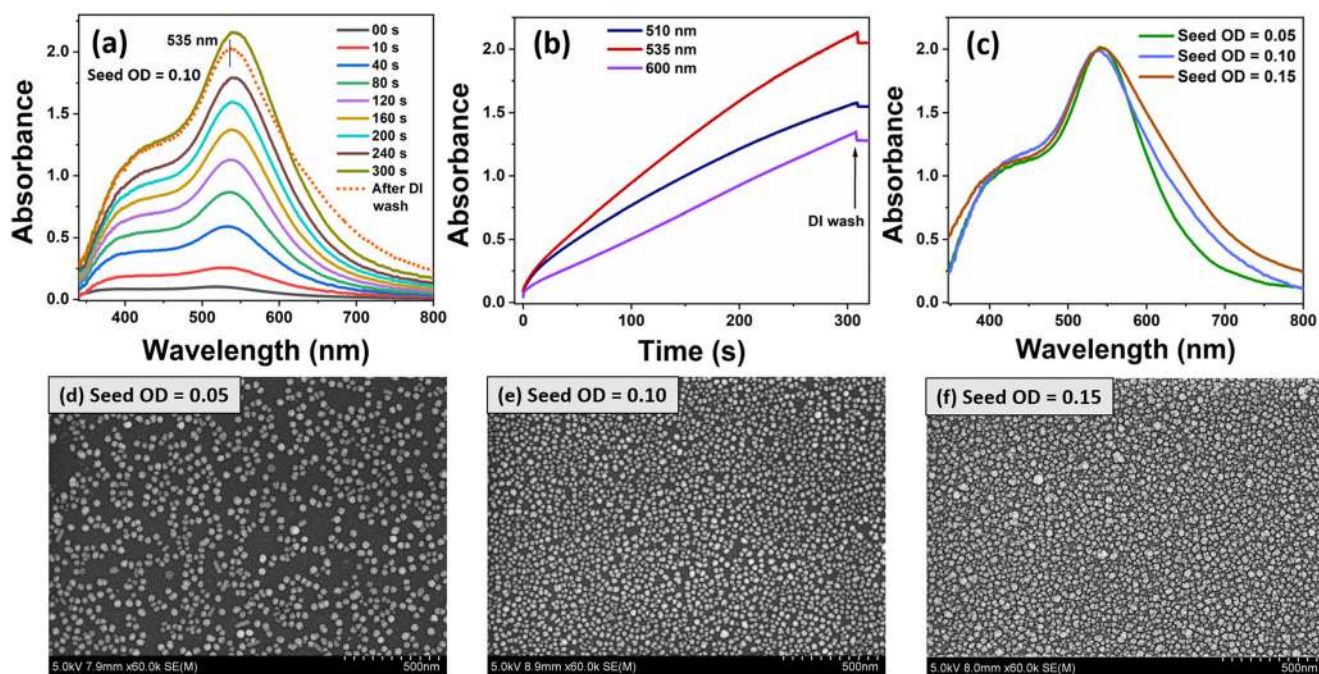

Fig. 3 Au seed–mediated growth of AuNPs on a U-bent FOS probe. **a** EWA-based spectra obtained at different time intervals during the AuNP growth (Au seed OD = 0.1). **b** Continuous real-time monitoring of absorbance at different wavelengths, namely, 510, 535, and 600 nm. **c** EWA spectra of the AuNP grown over the probes immobilized with seed at different densities measured in terms of peak absorbance as 0.05, 0.10, and 0.15 OD. **d–f** The respective SEM images of AuNPs (scale bar 500 nm)
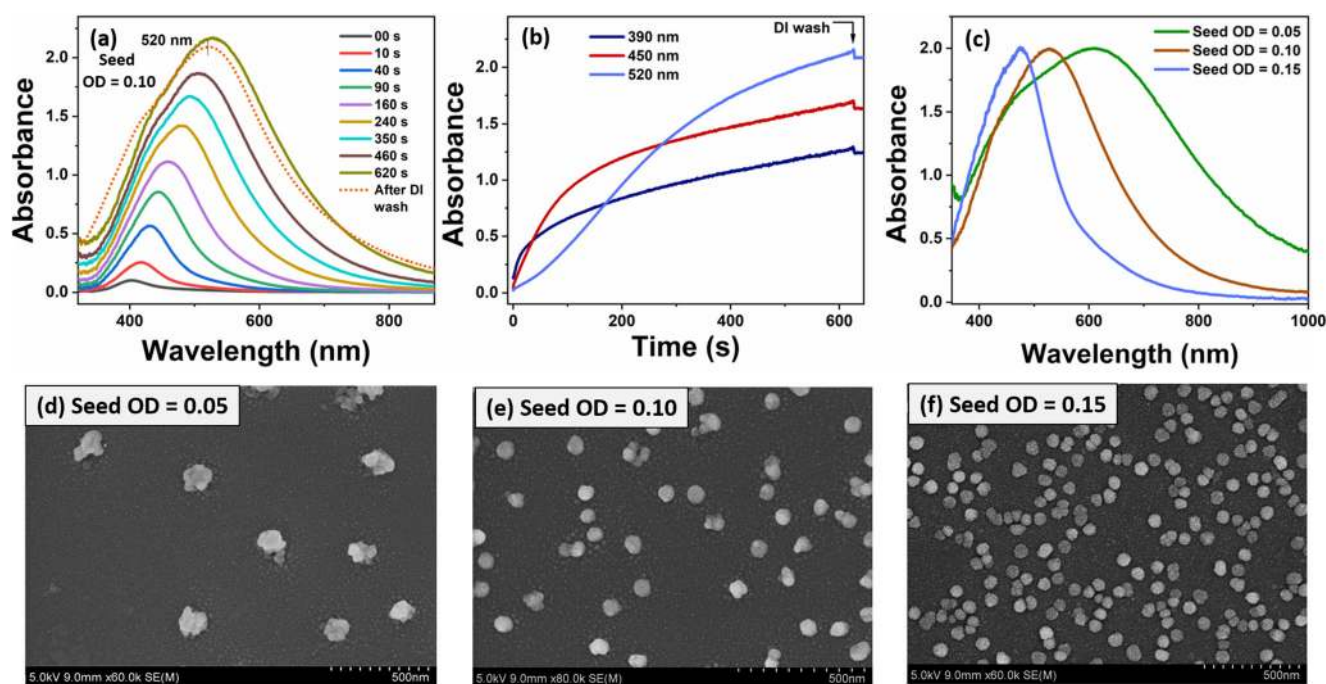
Fig. 4 Ag seed–mediated growth of AgNPs on a U-bent FOS probe. **a** EWA-based spectra obtained at different time intervals during the AgNP growth (Ag seed OD = 0.1). **b** Continuous real-time monitoring of absorbance at different wavelengths, namely, 390, 450, and 520 nm. **c** EWA spectra of the AgNP grown over the probes immobilized with seed at different densities measured in terms of peak absorbance as 0.05, 0.10, and 0.15 OD. **d**–**f** The respective SEM images of AgNPs (scale bar 500 nm)

formation of relatively large AgNPs with a height of 91 ± 9 nm. Form SEM images (Fig. 4d), the surface coverage of AgNPs was found to be 22 ± 6 particles/μm^2. A less dense AgNP packing with uniform distribution was observed (Fig. S5b, supplementary information).

A different growth pattern was observed in the case of the other seed densities (Fig. 4c). A plasmonic peak at 605, 520, and 475 nm with a FWHM value of 425, 247, and 160 nm was observed for seed densities of 0.05, 0.10, and 0.15 OD, respectively. The plasmonic peak redshift and the FWHM values were inversely proportional to the seed density. The anisotropic growth is more evident from the SEM images (Fig. 4d–f) of the probes with seed density 0.05 OD, where the AgNPs are also significantly larger in comparison with the other two seed densities (given that the peak absorbance response of 2.0 after growth was taken as reference).

A comparison between the fiber optic probes with AuNPs and AgNPs shows a significantly lower density of NPs in the case of AgNPs, which is attributed to the higher extinction coefficient of Ag seeds. EDX analysis (Fig. S7 and Table S1, supplementary information) of AuNP- and AgNP-coated fiber surface showed the presence of bromine, confirming the CTAB capping over the NPs. Interestingly, the growth solutions at the end of each experiment were clear and transparent indicating that seeds were firmly attached on the surface without leaching from the probe surface. No NP growth was observed in the absence of seeds, confirming that seeds were essential to initiate the NP formation. Studies on

the seed density variation show larger NPs with lesser surface coverage and smaller NPs with higher surface coverage for lower and higher seed densities, respectively (attributed to the limited supply of precursors). Additionally, to evaluate the influence of the light either propagating through or refracted out of the bend portion of the fiber on NP growth kinetics, the same experiments were performed (initial seed OD = 0.1) in the absence of light (offline), and the spectra were recorded only at the end of 300 and 620 s for AuNP and AgNP probes, respectively. No considerable deviation in the spectral characteristics (Fig. S8, supplementary information) was observed, indicating that visible light had minimal or no effect on the NP growth kinetics. FOS probes with a seed density 0.1 OD were used in all subsequent studies.

LSPR Activity of the Plasmonic FOS Probes

The LSPR spectral characteristics of the plasmonic NPs grown on the FOS probes depend on their size, shape, composition, and inter-particle distance of NPs on the surface. More importantly, any change in the dielectric medium surrounding the NPs induces a shift in the extinction properties of the NPs [31]. This property of NPs is extremely useful in sensing the local refractive index changes in the microenvironment of the NPs. To evaluate the RI sensitivity, AuNP and AgNP grown FOS probes were dipped in sucrose solutions with increasing RI values ranging from 1.333 to 1.348 RIU with a step increase of 3 milli-RIU. Figure 5a and b represent

Fig. 5 LSPR-based RI sensitivity measurements. Absorbance spectral response from **a** AuNP and **b** AgNP grown FOS probes in the presence of sucrose solutions of increasing RI value. **c** Plasmon peak absorbance response from bare and plasmonic FOS probes for RI changes in the medium from 1.333 to 1.348 RIU. **d** Comparison of RI sensitivities of bare and plasmonic FOS probes obtained from liner regression fits
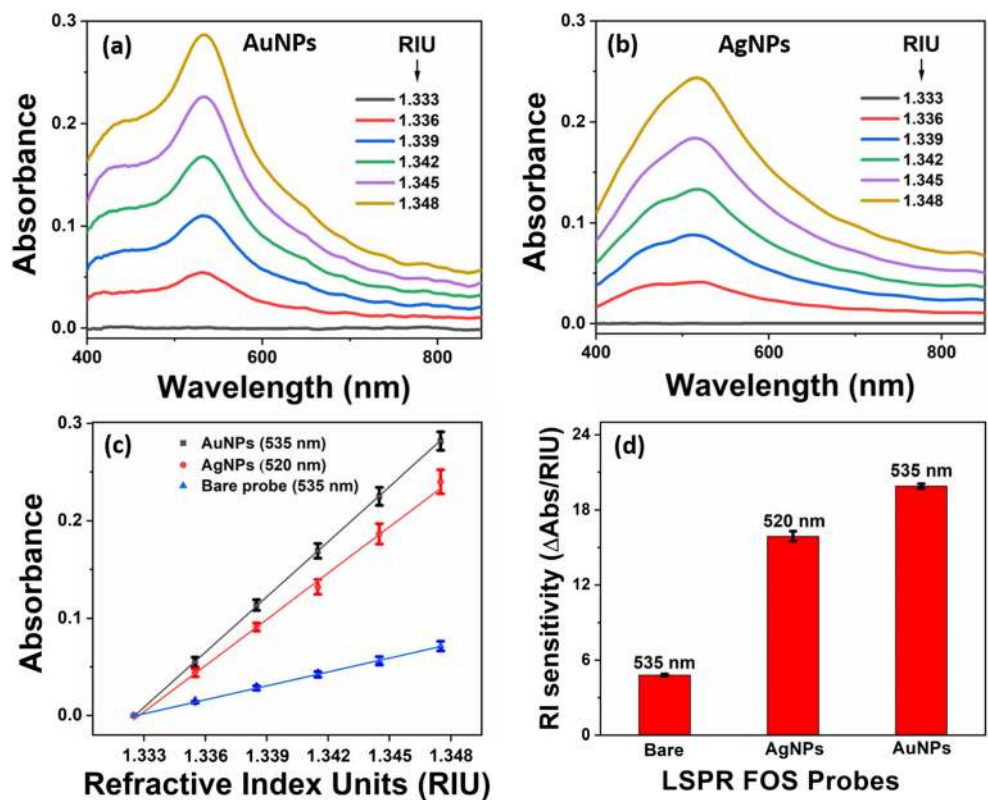
the LSPR spectral response obtained from AuNP and AgNP grown FOS probes, respectively. A significant increase in the absorbance spectral response was observed with the RI of the medium with a plasmon peak at 535 nm and 520 nm for AuNPs and AgNPs, respectively. RI sensitivity was defined as the ratio of absorbance response (ΔA at peak wavelength) to change in RIU surrounding the nanoparticles. Figure 5 c shows the peak absorbance response obtained from bare (without nanoparticles), AuNP (1424 particles/μm^2), and AgNP (22 particles/μm^2) grown FOS probes against the refractive index values. RI sensitivity was estimated from the slope of a linear regression fit. The RI sensitivity was found to be 18.9, 15.8, and 4.7 ΔA/RIU for AuNPs ($R^2 = 0.999$), AgNPs ($R^2 = 0.997$), and bare ($R^2 = 0.999$) probes, respectively (Fig. 5d). The RI sensitivity of AuNP probes was at least 7 to 9 times higher than nanopatterned gold-coated fiber probes fabricated using focused ion beam deposition technique reported elsewhere [32]. This RI sensitivity result obtained in this study was for probes with initial seed density of 0.1 OD. Additionally, the RI sensitivity can be improved by fine tuning the size, shape, and the number of AuNPs and AgNPs by identifying the optimum seed density and growth conditions.
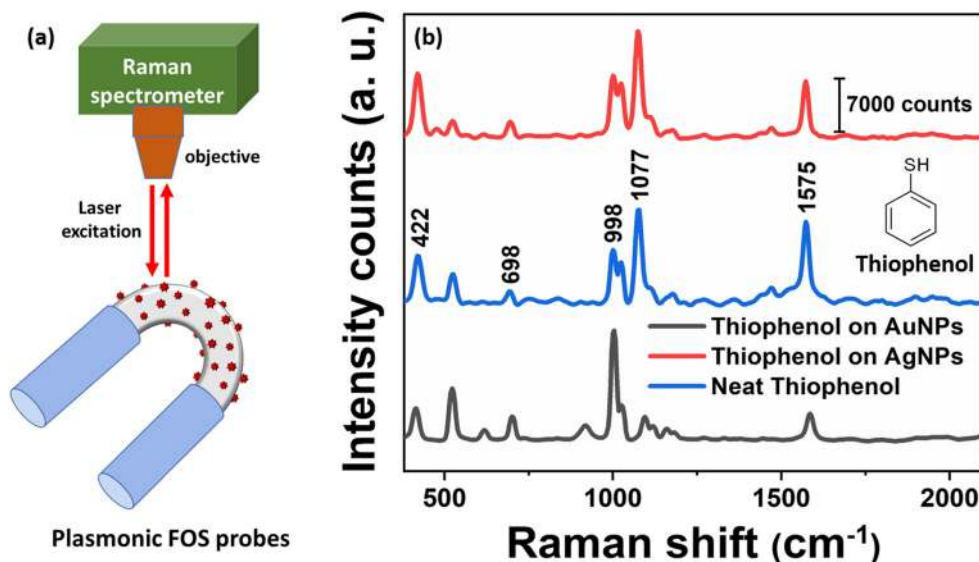
SERS Activity of the Plasmonic FOS Probes

U-bent FOS probes coated with plasmonic nanostructures offer a significant advantage of evanescent wave-based excitation of all the SERS active sites simultaneously unlike the conventional point-based measurements [33]. In addition, sampling issues can be minimized by simply dipping the tip of the probe into a small sample volume to allow adsorption of the analytes of interest rather than drop-casting of samples on conventional flat SERS substrates. With an appropriate optical instrumentation for efficient collection of Raman scattered photons from the fiber probes, the simultaneous excitation of the entire SERS-active substrate as well as the ease in handling of samples, the SERS-active U-bent FOS probes could be invaluable for chemical and biosensing applications [34].

In this study, however, a simple setup consisting of a Raman spectrometer integrated with a 785-nm laser was used to evaluate the SERS activity and estimate the enhancement factors of AuNP and AgNP FOS probes. Thiophenol was used as Raman label and a self-assembled monolayer was obtained on the NP surface. The fiber surface was brought to the focal point of the laser and spectrometer (Fig. 6a) to acquire the Raman scattering spectra from neat thiophenol, AuNP, and AgNP grown probes. SERS spectra from the thiophenol molecules adsorbed to the plasmonic probes were obtained as shown in Fig. 6b. Raman scattering spectral characteristic peaks at 422, 698, 998, 1022, 1077, and 1575 cm^{-1} were observed corresponding to C–S stretching; C–H out of plane deformation; S–H bending with in-plane ring deformation, in-plane deformation; C–S stretching with in-plane deformation; and C–C stretching modes, respectively [35]. Enhancement

Fig. 6 a Schematic representation of SERS measurements using a Raman spectrometer. **b** Characteristic SERS spectra (intensity) of thiophenol that was adsorbed on AuNPs, AgNP fiber probes, and neat thiophenol

factors (EF) for the SERS activity of plasmonic probes were estimated by using the following equation:

$$EF = (I_{SERS} \times N_{Raman})/(I_{Raman} \times N_{SERS})$$

where I_{SERS} and I_{Raman} are the Raman scattering intensities at a characteristic Raman shift of thiophenol on nanoparticles and Raman intensity from bulk solution (neat), respectively, normalized with respect to the laser optical power incident over a unit area and the spectral acquisition time. N_{SERS} and N_{Raman} are the corresponding number of thiophenol molecules bound to the plasmonic probe and a neat thiophenol solution, respectively, excited by the laser over the cross-sectional area of the laser spot. EFs for AuNP and AgNP grown FOS probes were estimated from the respective Raman scattering spectral intensities at 1575 cm^{-1}.

N_{Raman}, calculated from a thiophenol droplet on a cover slip exposed to 70-μm laser spot at the center, was 1.1×10^{-8} mol. N_{SERS} for AuNP and AgNP grown fiber probes was calculated by assuming a self-assembled monolayer of thiophenol molecules with a density of 0.71 and 0.5 nmol/cm^2 over the gold and silver surface, respectively [36, 37]. The NP size and density over the probes with a seed density of 0.1 OD were taken as mentioned previously. EF with respect to 1575 cm^{-1} was calculated to be 1.1×10^6 and 1.3×10^7 for AuNP and AgNP grown fiber probes, respectively. Detailed calculations for EF are described in supplementary information. The enhancement factor for AuNP grown probes is comparable with that of gold optical antennas on optical fibers fabricated by focused ion beam method [38]. Further, in an optrode configuration, using evanescent wave excitation, these plasmonic fiber probes can

Fig. 7 Stability of AuNPs (**a**) and AgNPs (**b**) grown over the fibers evaluated by subjecting them to hydrochloric acid, sodium hydroxide, hexane, and DI water over an hour and simultaneously recording the temporal absorbance response at 535 and 520 nm, respectively. All the probes had an initial peak absorbance of 2.0 OD
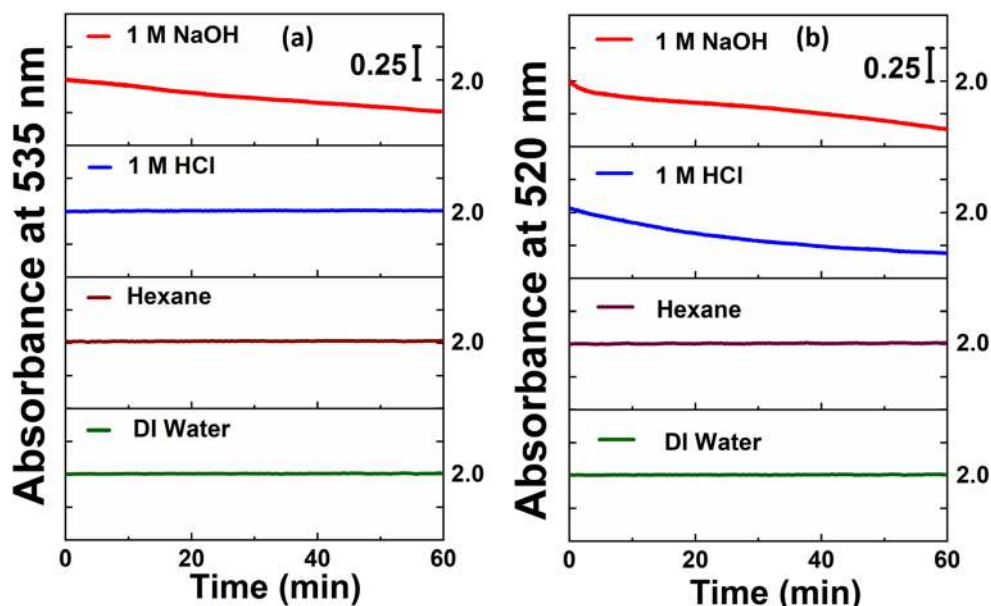
be used for remote SERS detection [39]. Hence, these seed-mediated plasmonic FOS probes can be a potential alternative for a cost-effective SERS platform.

Chemical Stability of Nanostructures

Plasmonic nanoparticles immobilized on a substrate are prone to desorption under harsh chemical conditions, and hence, it imposes a severe constraint on their utility in LSPR- and SERS-based applications [40–42]. To evaluate the chemical stability, freshly prepared AuNP and AgNP grown individual FOS probes (amine-functionalized) were separately immersed in DI water, hexane, HCl (1 M), or NaOH (1 M) for 1 h. Changes in the LSPR peak (absorbance peak) of the nanoparticles were monitored in real time. The temporal response (Fig. 7a, b) shows that both AuNP and AgNP FOS probes were stable for 1 h in DI water and hexane. In HCl solution (acidic), AuNPs were found to be highly stable. However, AgNP FOS probes showed 18% decrement in initial absorbance. Further, in NaOH solution, (alkaline), both AuNP and AgNP probes were found to have 12.5% and 18% decrement in their initial absorbance, respectively. UV-visible spectra and SEM images (Fig. S9 and 10, supplementary information) confirmed that the drop-in absorbance is due to desorption of nanoparticles from the amine-functionalized FOS surface. This stability studies reveal that the nanoparticle grown FOS probes may be suitable for sensing and biosensing applications except at extreme pH conditions such as pH 0 or pH 14.

Conclusion

In this study, we demonstrated a rapid and versatile seed-mediated technique to grow gold or silver nanoparticles on fiber optic probes for LSPR-based sensing applications. This in situ method of growing nanoparticles on the fiber probe offers remarkable real-time control to precisely manipulate the seed density and growth kinetics and thus their plasmonic properties. Since the size and surface chemistry of seeds and the composition of growth solution play a crucial role in determining the final shape of nanoparticles, this in situ seed-mediated growth technique facilitates a greater scope to synthesize a wide range of anisotropic nanoparticles on the fiber surface which may not be possible in solution phase due to aggregation issues.

References

1. Lal S, Link S, Halas NJ (2007) Nano-optics from sensing to waveguiding. Nat Photonics 1:641–648. https://doi.org/10.1038/nphoton.2007.223
2. Caucheteur C, Guo T, Albert J (2015) Review of plasmonic fiber optic biochemical sensors: improving the limit of detection. Anal Bioanal Chem 407:3883–3897. https://doi.org/10.1007/s00216-014-8411-6
3. Polley N, Basak S, Hass R, Pacholski C (2019) Fiber optic plasmonic sensors: providing sensitive biosensor platforms with minimal lab equipment. Biosens Bioelectron 132:368–374. https://doi.org/10.1016/j.bios.2019.03.020
4. Yin M j, Gu B, An QF et al (2018) Recent development of fiber-optic chemical sensors and biosensors: mechanisms, materials, micro/nano-fabrications and applications. Coord Chem Rev 376:348–392. https://doi.org/10.1016/j.ccr.2018.08.001
5. Long F, Zhu A, Shi H, Sheng J, Zhao Z (2015) Adsorption kinetics of pesticide in soil assessed by optofluidics-based biosensing platform. Chemosphere 120:615–620. https://doi.org/10.1016/j.chemosphere.2014.09.072
6. Mishra SK, Tripathi SN, Choudhary V, Gupta BD (2015) Surface plasmon resonance-based fiber optic methane gas sensor utilizing graphene-carbon nanotubes-poly(methyl methacrylate) hybrid nanocomposite. Plasmonics 10:1147–1157. https://doi.org/10.1007/s11468-015-9914-5
7. Huang Y, Zhu W, Li Z, Chen G, Chen L, Zhou J, Lin H, Guan J, Fang W, Liu X, Dong H, Tang J, Guan H, Lu H, Xiao Y, Zhang J, Wang H, Chen Z, Yu J (2018) High-performance fibre-optic humidity sensor based on a side-polished fibre wavelength selectively coupled with graphene oxide film. Sensors Actuators B Chem 255:57–69. https://doi.org/10.1016/j.snb.2017.08.042
8. Zhao Y, Lei M, Liu SX, Zhao Q (2018) Smart hydrogel-based optical fiber SPR sensor for pH measurements. Sensors Actuators B Chem 261:226–232. https://doi.org/10.1016/j.snb.2018.01.120
9. Srivastava SK, Gupta BD (2010) Resonance-based Fiber optic temperature sensor. America (NY) 27:1743–1749. https://doi.org/10.1364/JOSAA.27.001743
10. Velázquez-González JS, Monzón-Hernández D, Moreno-Hernández D, Martínez-Piñón F, Hernández-Romano I (2017) Simultaneous measurement of refractive index and temperature using a SPR-based fiber optic sensor. Sensors Actuators B Chem 242:912–920. https://doi.org/10.1016/j.snb.2016.09.164
11. Ricciardi A, Crescitelli A, Vaiano P, Quero G, Consales M, Esposito E, Cusano A (2015) Lab-on-fiber technology: a new vision for chemical and biological sensing. Analyst 140:8068–8079. https://doi.org/10.1039/c5an01241d
12. Dwivedi YS, Sharma AK, Gupta BD (2008) Influence of design parameters on the performance of a surface plasmon resonance based fiber optic sensor. Plasmonics 3:79–86. https://doi.org/10.1007/s11468-008-9058-y
13. Satija J, Punjabi NS, Sai VVR, Mukherji S (2014) Optimal design for U-bent fiber-optic LSPR sensor probes. Plasmonics 9:251–260. https://doi.org/10.1007/s11468-013-9618-7
14. Zamarreno CR, Matias IR, Arregui FJ (2012) Nanofabrication techniques applied to the development of novel optical fiber sensors based on nanostructured coatings. IEEE Sensors J 12:2699–2710. https://doi.org/10.1109/JSEN.2012.2199750
15. Sajanlal PR, Sreeprasad TS, Samal AK, Pradeep T (2011) Anisotropic nanomaterials: structure, growth, assembly, and functions. Nano Rev 2:5883. https://doi.org/10.3402/nano.v2i0.5883
16. Lohse SE, Burrows ND, Scarabelli L, Liz-Marzán LM, Murphy CJ (2014) Anisotropic Noble metal nanocrystal growth: the role of halides. Chem Mater 26:34–43. https://doi.org/10.1021/cm402384j

17. Langille MR, Personick ML, Zhang J, Mirkin CA (2012) Defining rules for the shape evolution of gold nanoparticles. J Am Chem Soc 134:14542–14554. https://doi.org/10.1021/ja305245g

18. Bakshi MS (2016) How surfactants control crystal growth of nanomaterials. Cryst Growth Des 16:1104–1133. https://doi.org/10.1021/acs.cgd.5b01465

19. Cao J, Galbraith EK, Sun T, Grattan KTV (2012) Effective surface modification of gold nanorods for localized surface plasmon resonance-based biosensors. Sensors Actuators B Chem 169:360–367. https://doi.org/10.1016/j.snb.2012.05.019

20. Aslan K, Lakowicz JR, Geddes CD (2005) Rapid deposition of triangular silver nanoplates on planar surfaces: application to metal-enhanced fluorescence. J Phys Chem B 109:6247–6251. https://doi.org/10.1021/jp044235z

21. Aslan K, Leonenko Z, Lakowicz JR, Geddes CD (2005) Fast and slow deposition of silver nanorods on planar surfaces: application to metal-enhanced fluorescence. J Phys Chem B 109:3157–3162. https://doi.org/10.1021/jp045186t

22. Wang Y, Tang L (2013) Chemisorption assembly of Au nanorods on mercaptosilanized glass substrate for label-free nanoplasmon biochip. Anal Chim Acta 796:122–129. https://doi.org/10.1016/j.aca.2013.08.024

23. Jana NR, Gearheart L, Murphy CJ (2001) Wet chemical synthesis of silver nanorods and nanowires of controllable aspect ratio. Chem Commun:617–618. https://doi.org/10.1039/b100521i

24. Jana NR, Gearheart L, Murphy CJ (2001) Wet chemical synthesis of high aspect ratio cylindrical gold nanorods. J Phys Chem B 105:4065–4067. https://doi.org/10.1021/jp0107964

25. Niu W, Zhang L, Xu G (2013) Seed-mediated growth of noble metal nanocrystals: crystal growth and shape control. Nanoscale 5:3172–3181. https://doi.org/10.1039/c3nr00219e

26. Bharadwaj R, Mukherji S, Mukherji S (2016) Probing the localized surface plasmon field of a gold nanoparticle-based fibre optic biosensor. Plasmonics 11:753–761. https://doi.org/10.1007/s11468-015-0106-0

27. Priyamvada VC, Ajina C, Radhakrishnan P (2018) Coating configuration dependency of fiber optic silver coated U-bent plasmonic sensor surfaces in concentration sensing measurements. Optoelectron Lett 14:465–469. https://doi.org/10.1007/s11801-018-8075-0

28. Spasopoulos D, Kazianris S, Karantzalis AE, Lidorikis E, Ikiades A, Kosmidis C (2017) Tailored aggregate-free Au nanoparticle decorations with sharp plasmonic peaks on a U-type optical fiber sensor by nanosecond laser irradiation. Plasmonics 12:535–543. https://doi.org/10.1007/s11468-016-0295-1

29. Christopher C, Subrahmanyam A, Sai VVR (2018) Gold sputtered U-bent plastic optical fiber probes as SPR- and LSPR-based compact plasmonic sensors. Plasmonics 13:493–502. https://doi.org/10.1007/s11468-017-0535-z

30. Link S, Wang ZL, El-Sayed MA (1999) Alloy formation of gold −silver nanoparticles and the dependence of the plasmon absorption on their composition. J Phys Chem B 103:3529–3533. https://doi.org/10.1021/jp990387w

31. Sepúlveda B, Angelomé PC, Lechuga LM, Liz-Marzán LM (2009) LSPR-based nanobiosensors. Nano Today 4:244–251. https://doi.org/10.1016/j.nantod.2009.04.001

32. Kim HM, Uh M, Jeong DH, Lee HY, Park JH, Lee SK (2019) Localized surface plasmon resonance biosensor using nanopatterned gold particles on the surface of an optical fiber. Sensors Actuators B Chem 280:183–191. https://doi.org/10.1016/j.snb.2018.10.059

33. Danny CG, Subrahmanyam A, Sai VVR (2018) Development of plasmonic U-bent plastic optical fiber probes for surface enhanced Raman scattering based biosensing. J Raman Spectrosc 49:1607–1616. https://doi.org/10.1002/jrs.5448

34. Wang C, Zeng L, Li Z, Li D (2017) Review of optical fibre probes for enhanced Raman sensing. J Raman Spectrosc 48:1040–1055. https://doi.org/10.1002/jrs.5173

35. Jung HY, Park YK, Park S, Kim SK (2007) Surface enhanced Raman scattering from layered assemblies of close-packed gold nanoparticles. Anal Chim Acta 602:236–243. https://doi.org/10.1016/j.aca.2007.09.026

36. Wan L-J, Terashima M, Noda H, Osawa M (2002) Molecular orientation and ordered structure of benzenethiol adsorbed on gold(111). J Phys Chem B 104:3563–3569. https://doi.org/10.1021/jp993328r

37. Schalnat MC, Pemberton JE (2010) Comparison of a fluorinated aryl thiol self-assembled monolayer with its hydrogenated counterpart on polycrystalline Ag substrates. Langmuir 26:11862–11869. https://doi.org/10.1021/la1010314

38. Sai VVR, Kundu T, Mukherji S (2009) Novel U-bent fiber optic probe for localized surface plasmon resonance based biosensor. Biosens Bioelectron 24:2804–2809. https://doi.org/10.1016/j.bios.2009.02.007

39. Ran Y, Strobbia P, Cupil-Garcia V, Vo-Dinh T (2019) Fiber-optrode SERS probes using plasmonic silver-coated gold nanostars. Sensors Actuators B Chem 287:95–101. https://doi.org/10.1016/j.snb.2019.01.167

40. Chen H, Zhao L, Chen D, Hu W (2015) Stabilization of gold nanoparticles on glass surface with polydopamine thin film for reliable LSPR sensing. J Colloid Interface Sci 460:258–263. https://doi.org/10.1016/j.jcis.2015.08.075

41. Suzuki S, Yoshimura M (2017) Chemical stability of graphene coated silver substrates for surface-enhanced Raman scattering. Sci Rep 7:1–7. https://doi.org/10.1038/s41598-017-14782-2

42. Lin XM, Cui Y, Xu YH, Ren B, Tian ZQ (2009) Surface-enhanced Raman spectroscopy: substrate-related issues. Anal Bioanal Chem 394:1729–1745. https://doi.org/10.1007/s00216-009-2761-5